In Vivo SPECT Quantification of Transplanted Cell Survival After Engraftment Using ^{111}In-Tropolone in Infarcted Canine Myocardium

Kimberley J. Blackwood[1,2], Benoit Lewden[1], R. Glenn Wells[3], Jane Sykes[1], Robert Z. Stodilka[1,2], Gerald Wisenberg[1,4], and Frank S. Prato[1,2]

[1]Imaging Program, Lawson Health Research Institute, London, Ontario, Canada; [2]Medical Imaging and Medical Biophysics Department, University of Western Ontario, London, Ontario, Canada; [3]Cardiac Imaging, University of Ottawa Heart Institute, Ottawa, Ontario, Canada; and [4]Division of Cardiology, London Health Sciences Centre, London, Ontario, Canada

Current investigations of cell transplant therapies in damaged myocardium are limited by the inability to quantify cell transplant survival in vivo. We describe how the labeling of cells with ^{111}In can be used to monitor transplanted cell viability in a canine infarction model. **Methods:** We experimentally determined the contribution of the ^{111}In signal associated with transplanted cell (TC) death and radiolabel leakage to the measured SPECT signal when ^{111}In-labeled cells were transplanted into the myocardium. Three groups of experiments were performed in dogs. Radiolabel leakage was derived by labeling canine myocardium in situ with free ^{111}In-tropolone ($n = 4$). To understand the contribution of extracellular ^{111}In (e.g., after cell death), we developed a debris impulse response function (DIRF) by injecting lysed ^{111}In-labeled cells within reperfused ($n = 3$) and nonreperfused ($n = 5$) myocardial infarcts and within normal ($n = 3$) canine myocardium. To assess the application of the modeling derived from these experiments, ^{111}In-labeled cells were transplanted into infarcted myocardium ($n = 4$; $3.1 \times 10^7 \pm 5.4 \times 10^6$ cells). Serial SPECT images were acquired after direct epicardial injection to determine the time-dependent radiolabel clearance. Clearance kinetics were used to correct for ^{111}In associated with viable TCs. **Results:** ^{111}In clearance followed a biphasic response and was modeled as a biexponential with a short ($T^s_{1/2}$) and long ($T^l_{1/2}$) biologic half-life. The $T^s_{1/2}$ was not significantly different between experimental groups, suggesting that initial losses were due to transplantation methodology, whereas the $T^l_{1/2}$ reflected the clearance of retained ^{111}In. DIRF had an average $T^l_{1/2}$ of 19.4 ± 4.1 h, and the $T^l_{1/2}$ calculated from free ^{111}In-tropolone injected in situ was 882.7 ± 242.8 h. The measured $T^l_{1/2}$ for TCs was 74.3 h and was 71.2 h when corrections were applied. **Conclusion:** A new quantitative method to assess TC survival in myocardium using SPECT and ^{111}In has been introduced. At the limits, method accuracy is improved if appropriate corrections are applied. In vivo ^{111}In imaging most accurately describes cell viability half-life if $T^l_{1/2}$ is between 20 h and 37 d.

Received Aug. 27, 2007; revision accepted Feb. 12, 2009.
For correspondence or reprints contact: Kimberley J. Blackwood, Lawson Health Research Institute, 268 Grosvenor St., London, ON, Canada, N6A 4V2.
E-mail: kblackwo@lawsonimaging.ca

Key Words: ^{111}In SPECT; cell transplant survival; myocardial infarction; canine bone marrow stromal cells; cell tracking

J Nucl Med 2009; 50:927–935
DOI: 10.2967/jnumed.108.058966

Although the prevalence of heart failure rises, current therapies inadequately address the pathophysiology leading to adverse myocardial tissue remodeling. Such remodeling can be activated by myocardial infarction (MI); ultimately, heart function deteriorates, initiating global dysfunction (*1–5*). To assess the treatment efficacy of cellular cardiomyoplasty, noninvasive and quantitative methods to track cell transplant survival in vivo are required (*6*). Of critical importance is improving cell survival and retention after transplantation by optimizing combinations of cell type (*6,7*), injection strategy (*6,7*), and injection time after infarction (*6–9*). Previous studies have demonstrated that cell delivery strategies affect the retention of cells in the myocardium (*10–12*). Therefore, a noninvasive method to quantify cell survival will help evaluate methods that aim to optimize survival, particularly within the first 2 wks after transplantation.

Noninvasive cell tracking technologies to determine cell survival, engraftment, and subsequent function require that existing imaging methodologies are optimized for sensitivity, specificity, and resolution of nondistributed sources. Numerous studies have imaged cell biodistribution and homing by directly labeling cells with radionuclides using SPECT and PET, which have sufficient sensitivity to detect nanomolar quantities (*6*) of γ-emitters in vivo. However, cellular quantification using these methods is complicated by radiolabel leakage from viable cells and clearance of radiolabeled cellular debris. Problems with significant radioisotope label leakage within the first hour have been reported with

^{18}F-FDG (*13–15*), ^{64}Cu-pyruvaldehyde bis(*N*4-methylthiosemicarbazone) (*13*), and ^{99m}Tc-hexamethylpropylene amine oxime (*14*). In addition to nuclear medicine techniques, MRI of contrast-labeled cells has been successful; however, sensitivity differences allow the detection of smaller amounts of contrast material using nuclear medicine techniques relative to MRI in large animal dual-labeling experiments (*5*).

The objective of this work was to demonstrate that ^{111}In-tropolone can monitor transplanted cell (TC) viability in a large animal model and that cell survival after transplantation in the canine myocardium can be estimated in vivo using radiolabeled cells and SPECT. The ^{111}In signal detected by SPECT corresponds to the sum of activity remaining within transplanted viable cells, released from dead cells, and leaked from viable cells. To correlate ^{111}In activity to viable cells, we hypothesized that by modeling the time-dependent clearance of ^{111}In at the injection site, we could remove the confounding radioactive signal attributed to activity within the volume of interest (VOI) but not contained within viable cells. Radiolabel leakage rate and clearance associated with transplanted cell death were acquired in vivo; these data were used to develop a corrected viable cell activity curve, demonstrating that ^{111}In cell labeling before myocardial transplantation can accurately estimate cell survival half-life between 20 h and 37 d.

MATERIALS AND METHODS

Stromal Cell Culture and Labeling

Canine studies were approved by the Animal Use Subcommittee at the University of Western Ontario. Three weeks before surgery, bone marrow was aspirated (10–15 mL) from the humerus of female mongrel dogs (20–25 kg; 1–2 y) after anesthesia was administered. Bone marrow mononuclear cells (BMMNCs) were isolated (Ficoll-Hypaque, 1.077 g/mL; Sigma) and plated in Dulbecco's Modified Eagle's Medium (DMEM) (Invitrogen) containing 10% fetal bovine serum and antibiotics (100 units of penicillin per milliliter and 100 μg of streptomycin per milliliter; Invitrogen). Cells were subsequently incubated (37°C, 5% CO_2) and floating cells were progressively washed away, leaving the adherent bone marrow stromal cell (BMSC) population that was subsequently culture-expanded for 3 wks. ^{111}In-tropolone cell labeling has been described previously (*16*). Briefly, BMSCs were incubated with ^{111}In-tropolone for 30 min at 37°C, and incubation was stopped by the resuspension of cells in 25 mL of DMEM, followed by centrifugation (430*g* for 5 min) and supernatant removal. Cells were washed again with phosphate-buffered saline (PBS), and the cell pellet was collected after centrifugation. The cell pellet (A) and supernatant including washes (B) were counted for ^{111}In activity using a dose calibrator (CRC-12; Capintec) to determine labeling efficiency (A/[A + B] × 100%).

Surgical Preparation

After anesthesia, a left thoracotomy was performed, exposing the anterior surface of the heart. In 12 of 19 dogs, MI was induced by placing a snare ligature around the left anterior descending coronary artery (LAD) distal to the first diagonal branch. After 2–3 h of occlusion, the LAD was either reperfused for 2–3 h by releasing the snare before injection or remained permanently occluded. Radiolabeled injections were performed as outlined below. Within 30–40 min of injection, the incision was closed and the animal was moved to the SPECT suite.

In Vivo Experiments

To determine the contributions of cell death, radiolabel leakage, and cell survival to the ^{111}In signal detected, 3 different in vivo experiments were performed.

To determine the contribution from cellular debris, approximately 1×10^7 BMMNCs ($n = 9$) or BMSCs ($n = 2$) were labeled in vitro with ^{111}In-tropolone and subjected to ultrasonication (Sonic Dismembrator 500; Fisher Scientific) continuously for 5 min to cause cell lysis. The cellular debris was injected into normal ($n = 3$) or infarcted canine myocardium that was either permanently occluded ($n = 5$) or reperfused ($n = 3$) for 2 h after 2 h of LAD occlusion. In the permanent occlusion group, cellular debris was injected into the infarct center; the reperfused infarct group received cellular debris injections within the infarct or normal border zone of the myocardium. From these experiments, the late ^{111}In kinetics from cellular debris is herein denoted as the debris impulse response function (DIRF).

Because cardiomyocytes have little turnover in normal tissue (*17–20*), canine myocardium was labeled in situ with ^{111}In-tropolone to determine clearance characteristics of ^{111}In from viable cells that did not die in vivo. Therefore, we hypothesized that labeling canine cardiomyocytes with ^{111}In-tropolone would provide an indication of radiolabel loss from cells that are not dying at an appreciable rate in normal myocardium. After thoracotomy, 4 dogs were injected with free ^{111}In-tropolone (mean ± SEM, 52.8 ± 17.1 MBq; 5–6 injections; 1 mL total volume) directly into the anterior surface of normal myocardium.

Finally, to obtain the total measured signal, viable BMSCs were injected in the peri-infarct region of reperfused infarcted myocardium. At the time of surgery, $3.08 \times 10^7 \pm 5.41 \times 10^6$ autologous canine BMSCs (3.69 ± 0.62 MBq; 1-mL volume; 5–7 injections) were intramyocardially injected ($n = 4$) after a 3-h LAD occlusion and reperfusion.

In Vitro Retention of ^{111}In in BMSCs

In 2 separate experiments, canine BMSCs (1.76×10^6) were radiolabeled with ^{111}In-tropolone, promptly plated, and incubated for 24 h to allow adhesion to culture plates. Supernatant activity containing ^{111}In released from viable cells was measured daily using a high-purity germanium well counter (GWL; Ortec), and cell activity was measured using a γ-camera (Millenium MG; GE Healthcare). In both experiments, static images of cells were collected consecutively for several days after radiolabeling. Before each imaging session, cells were rinsed twice with 5 mL of PBS and replenished with fresh medium. Old medium and rinses were collected and measured using the well counter. Cell counts were corrected for physical decay and background and were fit to a monoexponential curve to determine the ^{111}In biologic half-life for the imaging experiment. The cell viability after labeling and after the end of the experiments was assessed using trypan blue exclusion assay.

In Vitro Assessment of Nonspecific ^{111}In Uptake

Nonspecific ^{111}In uptake was assessed using the rat embryonic cardiomyoblast H9c2 cell line (CRL-1446; American Type Culture Collection), which served as an in vitro model of normal myocardium. To determine the uptake of ^{111}In released after cell

lysis, 1.3 × 10^6 BMSCs were labeled and lysed as described above. Radiolabeled lysates were then incubated with approximately 1 million H9c2 cells for 30 min, after which incubation activity was removed and cells were rinsed twice with 5 mL of PBS. Control H9c2 cells were labeled with ^{111}In-tropolone as described. Cells were then trypsinized and collected for measurement using the well counter. Rinses and incubation activity were also measured.

The uptake of ^{111}In lost from viable BMSCs by H9c2 cells was also evaluated. To do this, supernatant containing leaked ^{111}In activity was collected from ^{111}In-labeled BMSCs and incubated with H9c2 cells for 30 min. After incubation, the supernatant was removed and cells were rinsed with PBS and trypsinized. Counts from cells, supernatant, and rinses were measured using the well counter. Control H9c2 cells were labeled with ^{111}In-tropolone.

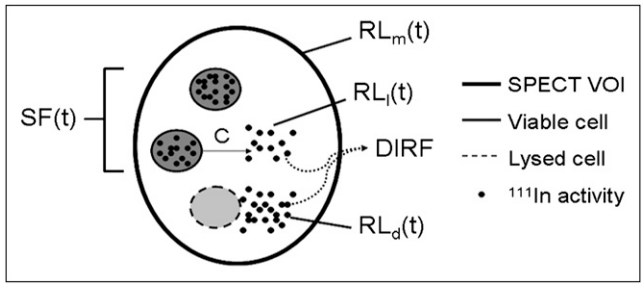

FIGURE 1. SPECT VOI (RL$_m$(t)) containing radiolabel released from dead cells (RL$_d$(t)), leaked from viable cells (RL$_l$(t)) (C is fractional loss from viable cells), and in viable cells (SF(t)). DIRF describes kinetics of ^{111}In after cell death.

SPECT Image Acquisition and Image Analysis

Serial SPECT and whole-body images were alternately acquired on anesthetized dogs using a dual-head Millennium MG equipped with medium-energy parallel-hole collimators. SPECT parameters were a 128 × 128 pixel matrix (4.52 mm^2/pixel), 64 projections per head acquired over 180° (total 128 projections over 360°), and 171 and 245 keV (±10%) ^{111}In energy windows. Whole-body imaging parameters were a 256 × 1,024 pixel matrix (with 2.26 mm^2/pixel), a fixed acquisition time of 23 min, and the same ^{111}In energy windows that were used for SPECT. SPECT and whole-body images of cellular debris and free ^{111}In-tropolone injections were imaged serially on the day of injection; additional follow-up imaging was done for the free ^{111}In-tropolone and viable cell injections over 3 and 2 wks, respectively. Subsequent follow-ups for these experiments required progressively longer SPECT image acquisitions of 30, 60, and 180 s/projection to obtain adequate count statistics in response to the decrease in the ^{111}In signal.

SPECT projections were corrected for background and reconstructed using an iterative algorithm (*21*). VOI analysis was conducted on reconstructed SPECT images to generate time–activity curves, which were corrected for physical decay. In this analysis, the first SPECT dataset acquired (t = 0) had a VOI defined as pixels greater than or equal to 30% of the maximum pixel intensity and was used to create a mask image. This mask was then multiplied by each SPECT image acquired, and the mean pixel intensity was determined (MATLAB; MathWorks). Time–activity curves were fit to a biexponential function using MATLAB, and the short ($T^s_{1/2}$) and long ($T^l_{1/2}$) components of the clearance curves were determined. Experiments involving viable BMSC transplantations were analyzed such that the last 3 data points were fit to a monoexponential function, and the resulting half-life was reported as the $T^l_{1/2}$.

Modeling Transplanted Cell Viability Kinetics

To quantify the kinetics of TC survival within a VOI, we begin by stating that at any time, t, the total radiolabel signal measured (RL$_m$(t)) by SPECT within the VOI comprises radiolabel released from dead TCs that remain in the VOI, RL$_d$(t); radiolabel released from live TCs that remain in the VOI, RL$_l$(t); and radiolabel within the surviving fraction of viable TCs, SF(t) (Fig. 1). We express each of these quantities in terms of the initial number of TCs (NTC) and the amount of radiolabel per TC at time 0, RL$_{PTC}$. Additionally, RL$_m$(t) is normalized to the sensitivity of the imaging system per TC and corrected for the radioactive decay of the radiolabel. Thus:

$$RL_m(t)\times NTC\times RL_{PTC} = [SF(t)+RL_d(t)+RL_l(t)]\times NTC\times RL_{PTC}. \quad \text{Eq. 1}$$

Equivalently:

$$SF(t) = RL_m(t) - RL_d(t) - RL_l(t), \quad \text{Eq. 2}$$

where each term ranges between 0 and 1. Our objective is to determine the shape of SF(t), which cannot be measured directly.

First, we assume a functional form for the surviving fraction of TC, SF(t):

$$SF(t) = \exp\left(-\frac{\ln 2}{T_{SF}}t\right), \quad \text{Eq. 3}$$

where the half-life, T$_{SF}$, is what we ultimately seek. We similarly assume a functional form for RL$_m$(t):

$$RL_m(t) = \exp\left(-\frac{\ln 2}{T_m}t\right), \quad \text{Eq. 4}$$

where T$_m$ is the biologic half-life of the SPECT time–activity curve.

The term RL$_d$(t) in Equation 2 considers radioactive label released from dead TCs and the removal of that label from the VOI. To account for this effect, we consider the number of TCs that have died from time 0 to time t, radioactive label—or debris—released from each dead cell, and kinetics of the debris retention at, and clearance from, the VOI. More formally:

$$RL_d(t) = \int_0^t [SF(\tau - d\tau) - SF(\tau)]\otimes DIRF(t-\tau)d\tau, \quad \text{Eq. 5}$$

where SF(τ − dt) − SF(τ) describes the rate of change of SF(t) around time τ, DIRF(τ) is the DIRF at time τ, and ⊗ represents the convolution operator. Here, we assume that all radioactive label is released instantaneously on cell death—hence becoming debris—and immediately begins to clear from the VOI according to the kinetics of DIRF.

The final term in Equation 2, $RL_l(t)$, describes radiolabel leakage from surviving TCs, where leakage refers to the removal of ^{111}In by any number of mechanisms, followed by subsequent clearance from the VOI according to DIRF. Thus:

$$RL_l(t) = C\int_0^t SF(\tau)\otimes DIRF(t-\tau)d\tau, \qquad \text{Eq. 6}$$

where the constant C describes the proportion of radiolabel inside a TC that leaves the TC and then begins to be cleared. Further, although the clearance of radiolabeled debris from dead cells may differ from radiolabel leaked from surviving cells, we have made the assumption that the clearance mechanism will be similar within the same tissue.

With $RL_d(t)$ and $RL_l(t)$ determined, we can correct the measured $RL_m(t)$ for the confounding effects of radiolabel from dead TCs and radiolabel leakage from the surviving fraction of TCs, thereby isolating the TC survival curve. More specifically, we determined the surviving fraction half-life, T_{SF}, using a least-squares fit:

$$T_{SF} = \arg\min_{t_{SF}} \int \left\{ \exp\left(-\frac{\ln 2}{T_m}t\right) - \left[\exp\left(-\frac{\ln 2}{t_{SF}}t\right) + RL_d(t) + RL_l(t)\right]\right\}^2 dt, \qquad \text{Eq. 7}$$

where the time integral is taken over the SPECT experimental time. Equation 7 was solved using the Marquardt–Levenberg iterative search algorithm, as implemented in MATLAB.

We constructed a plot of T_{SF} versus T_m to better appreciate the significance of the correction obtained by Equation 7. Using this plot, we estimated the TC survival curve half-life based on the radiolabel time–activity curve measured by SPECT. The T_{SF} versus T_m plot has a minimum bound on T_m, defined as the variability of the half-life of DIRF because no radiolabel can clear faster than extracellular radiolabeled debris, and a maximum bound on T_m, defined by the variability in the half-life of the clearance of radiolabel from viable cells.

Experiments to measure DIRF(t) were repeated multiple times. Rather than averaging multiple DIRF curves, each DIRF curve was input individually to Equation 7, thus providing a range of possible T_{SF} values for a given T_m. For a particular T_m, only those DIRF curves clearing faster than that T_m were considered to produce corresponding T_{SF} values, which were then averaged and their SD calculated.

Statistical Analysis

Statistical analysis was performed using SPSS 15.0 (SPSS Inc.). Nonparametric tests were used for in vivo data that were not normally distributed, with corrections made for multiple pairwise comparisons. For cellular debris data, differences between injected tissue type (nonreperfused, normal, and reperfused) were determined using 2-way ANOVA. A 2-tailed test of significance detected differences between groups (significance set at $\alpha = 0.05$). In vitro studies were analyzed using unpaired *t* tests, and exponential fits to in vivo data were assessed with goodness-of-fit statistics in MATLAB. All values are expressed as mean ± SEM unless otherwise indicated.

RESULTS

In Vitro Retention of ^{111}In in BMSCs

BMSC viability was 93% after radiolabeling and had a labeling efficiency of 92%. After incubation activity was removed and cells were washed, the cellular ^{111}In activity was 0.105 Bq/cell. Imaging revealed that retained ^{111}In activity had a 14.1-d half-life (Supplemental Fig. 1; supplemental materials are available online only at http://jnm.snmjournals.org), and the subsequent viability at day 6 was 75%. Initial losses of ^{111}In from viable BMSCs between days 0 and 1 were 17.6%; the average loss was 4.6% per day thereafter. Two independent experiments confirmed these results.

In Vitro Assessment of Nonspecific Uptake of ^{111}In

We determined whether activity from lysed cells labeled surrounding cells with intact cell membranes in vitro. The inability of intact viable cells to take up ^{111}In released from lysed cells after a 30-min incubation period was demonstrated. Figure 2A shows uptake of ^{111}In from cellular debris in H9c2 cells, which had a labeling efficiency of 0.6% after the removal of ^{111}In-labeled BMSC debris (52.2 ± 2.4 counts per second [cps] vs. 8,357.4 ± 837.1 cps; $P < 0.01$). The control cell group labeled with ^{111}In-tropolone alone had a labeling efficiency of 68%. Similarly, ^{111}In released by viable BMSCs and incubated with H9c2 cells demonstrated significantly less ^{111}In associated with H9c2 cells, compared with the supernatant (0.79 ± 0.14 cps vs. 40.38 ± 0.86 cps; $P < 0.001$), as shown in Figure 2B.

In Vivo Acquisition of DIRF, $RL_l(t)$, and $RL_m(t)$

Cellular debris experiments showed faster radiolabel clearance curves when injected under the same conditions as viable cells. Figure 3A shows time–activity curves from which $T^s_{1/2}$ and $T^l_{1/2}$ (i.e., DIRF) (Fig. 3B) for all cellular debris experiments were derived, giving values of 1.75 ± 0.36 h and 19.37 ± 4.05 h, respectively. When results were separated into infarcted and normal tissue injections, the $T^s_{1/2}$ and $T^l_{1/2}$ were not significantly different between these groups; this was also true for groups separated on the basis

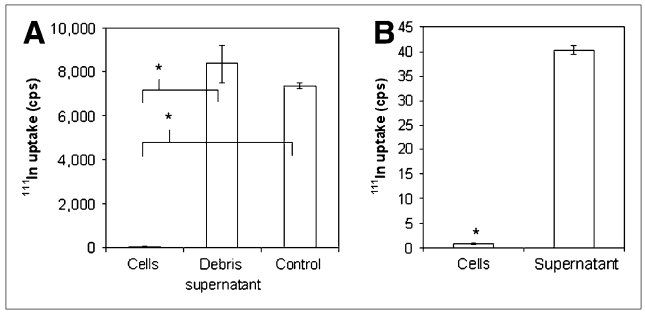

FIGURE 2. Nonspecific uptake of ^{111}In in H9c2 cardiomyoblasts. (A) After incubation of ^{111}In-labeled BMSC cellular debris with H9c2 cells, compared with control H9c2 cells labeled with ^{111}In-tropolone, no significant uptake of ^{111}In in H9c2 cells was found ($P < 0.001$). (B) Evaluation of nonspecific uptake of ^{111}In leaked from viable BMSCs indicated that significant amount of ^{111}In remained within incubating supernatant, compared with H9c2 cells ($P < 0.01$).

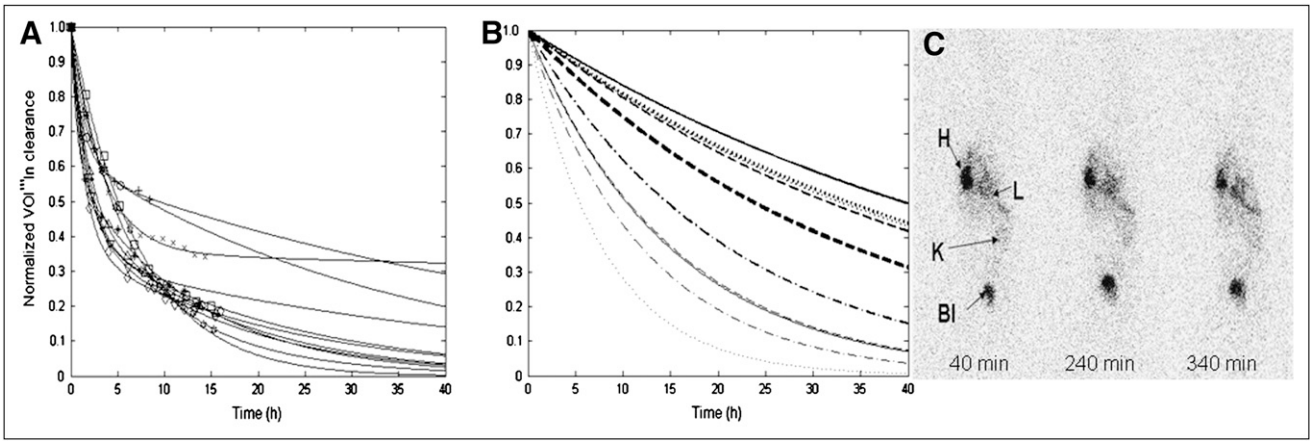

FIGURE 3. (A) Biexponential fits to time–activity curves (symbols represent normalized raw data) after injection of ^{111}In-labeled cellular debris into canine myocardium (normal, reperfused, and nonreperfused; n = 11). (B) DIRF as calculated from long component of biexponential fits ($T^{l}_{1/2}$ = 19.4 ± 4.1 h). (C) Whole-body scans from 1 dog injected with ^{111}In-labeled cellular debris in peri-infarct region of infarcted myocardium. All images are scaled to maximal pixel count and qualitatively demonstrate biodistribution of labeled debris within injected heart (H), liver (L), kidneys (K), and bladder (Bl).

of cellular debris injected into reperfused or permanent infarctions. Figure 3C shows whole-body scans acquired at approximately 40, 240, and 340 min after the injection of ^{111}In-labeled cellular debris into the infarcted myocardium of 1 dog, demonstrating ^{111}In reduction in the heart and increased bladder activity over time.

In experiments to determine ^{111}In radiolabel leakage from cells that do not die, in situ labeling of host cardiomyocytes showed similar washout characteristics for $T^{s}_{1/2}$, whereas the $T^{l}_{1/2}$ was longer than the $T^{l}_{1/2}$ from the cellular debris injections. Figure 4A shows the time–activity curves used to derive $T^{s}_{1/2}$ and $T^{l}_{1/2}$, which were calculated to be 1.34 ± 0.35 h and 882.66 ± 242.84 h, respectively. Figure 4B shows ^{111}In biodistribution in whole-body scans from 1 dog after the injection of free ^{111}In-tropolone in situ within normal myocardium on days 0, 7, and 15 and also demonstrates that most of the label remains within the injection site. Figure 4C is a SPECT/CT image showing the ^{111}In label after injection into the anteroapical region of normal myocardium. Contrast-enhanced MRI of the excised heart (Supplemental Fig. 2), used to confirm the absence of myocardial damage due to these injections, demonstrated no uptake of gadolinium-diethylenetriaminepentaacetic acid and indicated no myocardial damage 21 d after the injection of ^{111}In-tropolone in 2 dogs.

To determine $RL_m(t)$, canine BMSCs were injected into the myocardium and imaged with SPECT. The labeling efficiency was 73%, and average cellular activity was 0.12 ± 0.006 Bq/cell. Monoexponential fits to the data were good, and time–activity curves after viable BMSC

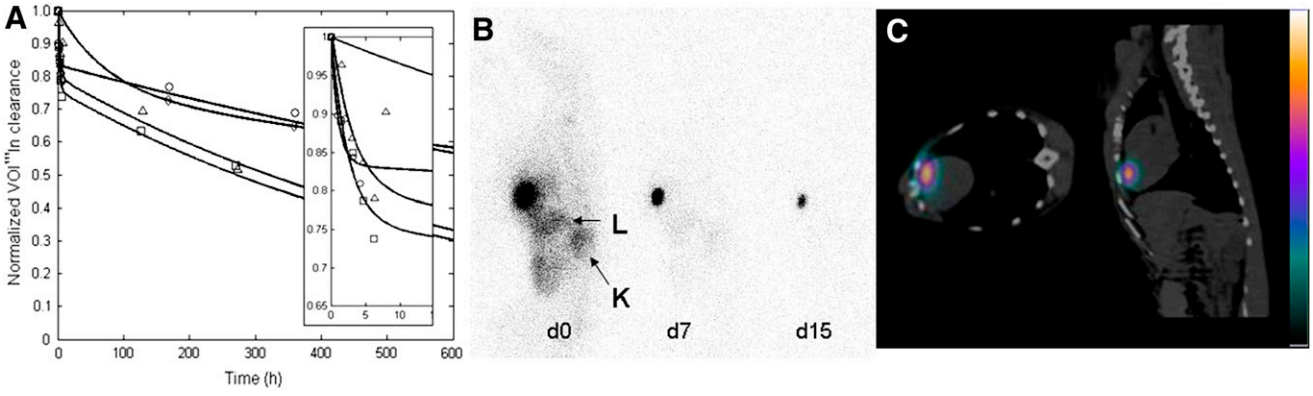

FIGURE 4. (A) Biexponential fits to SPECT time–activity curves after injection of ^{111}In-tropolone into normal canine myocardium ($T^{l}_{1/2}$ = 882.7 ± 242.8 h) (symbols represent normalized raw data). Dogs were serially imaged on injection day (see inset) and weekly thereafter. (B) Whole-body scans from 1 dog injected with ^{111}In-tropolone showing radiolabel in heart on days 0 (d0), 7 (d7), and 15 (d15). All images are scaled to maximal pixel value. (C) SPECT/CT image of ^{111}In radiolabel in normal myocardium of 1 dog localizing ^{111}In injection within heart in transaxial and sagittal planes, respectively. L = liver; K = kidneys.

transplantation in 4 dogs had an average $T^{l}_{1/2}$ of 74.25 ± 7.55 h, as shown in Figure 5A. Images show whole-body scans of 1 dog injected with ^{111}In-labeled BMSCs at days 3 and 7 after injection (Fig. 5B), with confirmation by SPECT/CT immediately after the injection (Fig. 5C) in an additional dog.

The measured biologic half-lives for all dogs in all groups are shown in Table 1.

Modeling Transplanted Cell Survival

The cellular debris experiments facilitated the determination of the kinetics of ^{111}In-labeled cellular debris from the SPECT VOI. The $T^{l}_{1/2}$ was used in the model to obtain the kinetics.

In observing the true leakage fraction (C) from viable TCs, the effects of DIRF kinetics were removed. Although the rate of ^{111}In clearance from the VOI was found to have an average leakage $T^{l}_{1/2}$ of 36.8 d, we assumed this was not the true leakage because we modeled ^{111}In outside viable TCs as clearing according to DIRF. Thus, the DIRF contribution was removed from the measured leakage clearance, and the adjusted leakage $T_{1/2}$ was 38.5 d with C calculated to be 0.00075/h.

The resulting T_m versus T_{SF} curve corrected for cell death and leakage to determine TC survival is shown in Figure 6. At longer half-lives, $RL_l(t)$ affected the accuracy of the true cell activity because leaked activity accumulated outside viable cells but had not yet been removed according to DIRF. At short half-lives, the average DIRF clearance of 19.4 ± 4.1 h resulted in delayed cellular debris washout from the myocardium, thus affecting how well the model predicted the activity within intact cells. Therefore, the most accurate estimation of the true cell activity was between approximately 20 h and 37 d. The measured T_m from the viable cell transplantations was 74.3 ± 7.6 h and after corrections became 71.2 ± 6.4 h using this curve.

DISCUSSION

We have developed a quantitative SPECT method to image canine BMSC survival in vivo after radiolabeling the cells with ^{111}In-tropolone and autologously transplanting them within the myocardium. In establishing this method, we had to determine the following: whether cellular ^{111}In levels caused radiotoxicity, the retention of ^{111}In in transplanted cells, the nonspecific uptake due to extracellular ^{111}In activity, and the clearance kinetics of the interstitial radiolabel.

Our previous work showed that loading BMSCs by as much as 0.14 Bq/cell did not affect viability at 14 d and proliferation at 5 d (*16*). Work by others examining cellular ^{111}In cytotoxicity (*5,22,23*) has suggested that greater amounts of ^{111}In per cell can be used. Dosing studies suggest that loading cells with 0.18 Bq/cell (*5*) or 7.5 Bq/cell (*23*) does not compromise cellular function. Loading human mesenchymal stem cells with 7.5 Bq/cell did not affect proliferation capacity, endothelial cell differentiation ability, and surface protein expression patterns over 5–7 d (*23*). Thus, the ^{111}In dose used here should produce minimal damage to canine BMSC function and viability. Although cellular fractionation studies have shown that ^{111}In-oxine is confined mostly to neutrophil cytoplasm (80% of total cellular activity) (*24*), the range of Auger electrons that accompany ^{111}In decay are in the nanometer to micrometer range (*25*). Thus, ^{111}In likely has minimal effect on radiation-sensitive compartments such as nuclear DNA. Indeed, it has been shown that translocation of ^{111}In, compared with cytosolic ^{111}In, to the nucleus of breast cancer cells severely affects cell survival (*26*).

Several challenges remain in quantitatively imaging cellular viability using a nonspecific radiotracer. Radiolabel leakage from viable cells and nonspecific radiolabel uptake in the extravascular and extracellular space affect quanti-

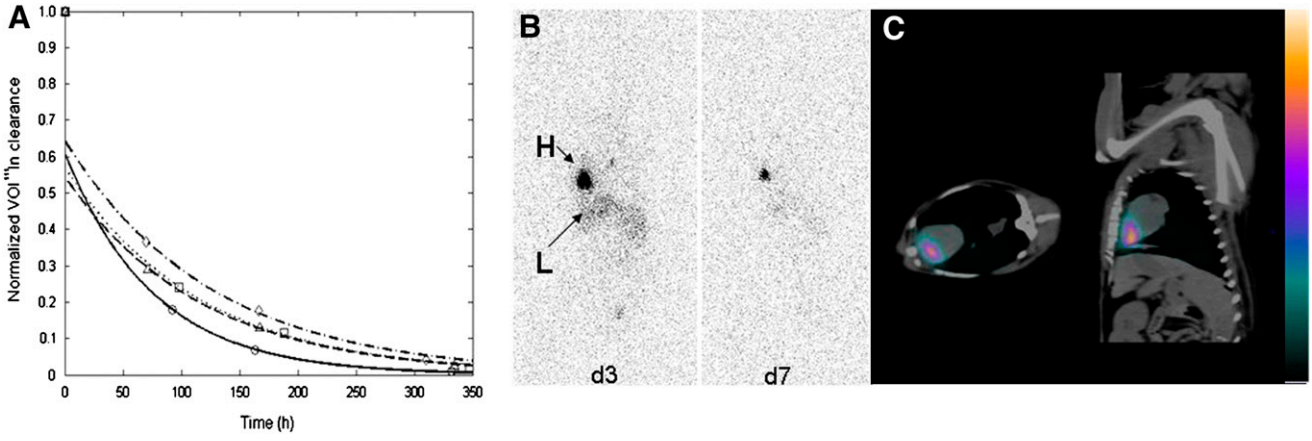

FIGURE 5. (A) SPECT time–activity curves showing long component of monoexponential fits for BMSC injections ($T^{l}_{1/2}$ = 74.3 ± 7.6 h) (symbols represent normalized raw data). (B) Whole-body scans from 1 dog injected with ^{111}In-labeled BMSCs within infarcted myocardium. Both images are scaled to maximal pixel count and show ^{111}In activity remaining in heart (H) and liver (L) at days 3 (d3) and 7 (d7) after injection. (C) SPECT/CT images confirm presence of BMSCs in myocardium on transplantation day.

TABLE 1. Biologic Half-Lives from Canine Experiments

Injection	Dog	Tissue	$T^s_{1/2}$ (h)	$T^l_{1/2}$ (h)
Cellular debris	1	N	1.282	1.282
	2		1.008	10.406
	3		1.083	39.745
			1.124 ± 0.082	17.144 ± 11.603
	4	R	1.237	10.615
	5		0.754	23.852
	6		1.378	31.752
			1.123 ± 0.188	22.073 ± 6.166
	7	C	1.081	14.664
	8		2.198	33.023
	9		4.834	5.466
	10		1.428	33.878
	11		3.070	8.377
			2.522 ± 0.672	19.082 ± 6.053
			1.759 ± 0.364 (58%)	19.369 ± 4.052 (42%)
In situ ^{111}In-tropolone	12	N	1.473	394.058
	13		1.867	536.077
	14		—*	1,305.854
	15		0.690	1,294.634
			1.344 ± 0.346 (18%)	882.66 ± 242.84 (82%)†
Viable BMSCs	16	R	—	79.544
	17		—	86.341
	18		—	78.955
	19		—	52.156
			—	74.249 ± 7.55‡

*Serial SPECT not acquired on injection day.

†$P < 0.001$ free ^{111}In-tropolone group vs. cellular debris group.

‡$P < 0.001$ transplanted BMSC group vs. cellular debris group.

N = normal myocardium; R = reperfused myocardium; C = permanently occluded myocardium.

Values are mean ± SEM. Percentages represent measured signal that clears with each specified half-life.

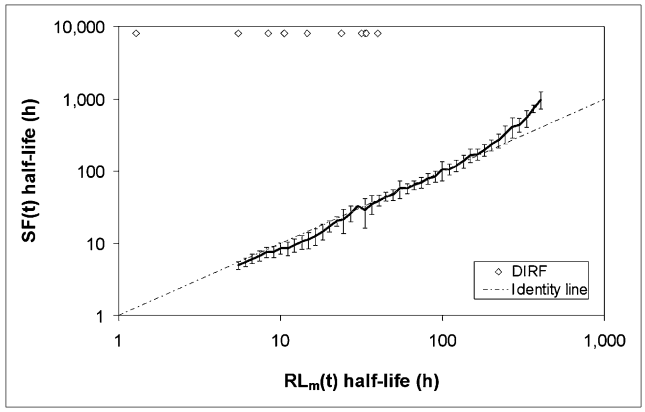

FIGURE 6. Plot of T_m vs. T_{SF} shows calculated half-life of surviving fraction of TCs after corrections for radiolabel leakage ($RL_l(t)$) and death ($RL_d(t)$) kinetics are made to apparent half-life measured by SPECT ($RL_m(t)$). Error bars represent SD, and ◇ represents incorporation of another DIRF curve in estimation of T_{SF}.

fication. Tran et al. (*27*) demonstrated that ^{111}In-oxine leakage from rat mesenchymal stem cells was initially high at 2 h after labeling but decreased by less than 1% per hour thereafter. ^{111}In leukocyte labeling was also evaluated for label stability and had elution rates of 2% per hour (*28*). Our in vitro results indicated similar levels of stability in canine BMSCs, with 4.6% of activity lost per day. We also demonstrated ^{111}In stability in viable cells in vivo. Because we were unable to control the viability of transplanted cells, we labeled endogenous cardiomyocytes in situ (because this population is largely postmitotic) (*20*). In these animals, $T^l_{1/2}$ was approximately 883 h, and ex vivo gadolinium-diethylenetriaminepentaacetic acid MRI confirmed the absence of myocardial damage due to these injections, suggesting ^{111}In labeling of intact viable myocardial cells. Cumulatively, these results suggest ^{111}In-tropolone was retained within viable cells and subsequently provided an estimate of radiolabel leakage. Our leakage rate collectively represents all putative fractions of myocardial tissue due to radiolabel nonspecificity; however, average rates of 1.8% per day suggest ^{111}In remains stable in viable cells. For quantitative imaging, we also needed to establish the extent to which ^{111}In might be nonspecifically taken up by surrounding tissue as a result of cell death or radiolabel lost from viable cells. We addressed this by showing that the ^{111}In from labeled stromal cellular debris was not significantly taken up by H9c2 cells in culture. Additional in vitro experiments also indicated that H9c2 cells incubated with leaked ^{111}In from viable BMSCs was not taken up by H9c2 cells. These data suggest that quantitative viable cell imaging will not be affected by nonspecific radiolabel uptake in the surrounding myocardium.

In vivo assessments of DIRF related to the time-dependent clearance of ^{111}In-labeled dead cellular debris from myocardium was essential in developing a quantitative imaging model to assess cell viability. Our results indicated an average $T^l_{1/2}$ of 19.4 h when labeled cellular debris was injected into normal and infarcted tissues. However, viable cells injected into infarcted myocardium cleared with a longer average $T^l_{1/2}$ of 74.3 h, suggesting the ability to distinguish between viable and dead cell injections with SPECT. As a result of the $T^l_{1/2}$ of cellular debris, convolution-based modeling was used to remove its contribution to the overall ^{111}In signal. Additionally, we tried to determine how myocardial blood flow might affect the DIRF by injecting labeled cellular debris into normal myocardium and infarcted myocardium that was either permanently occluded or reperfused but found no significant differences between these groups. Further investigation to accurately measure blood flow in more animals is warranted.

Our time–activity curve analysis revealed 2 distinct phases occurring with ^{111}In clearance from the VOI. Initially, we thought that the fast phase reflected viable cells dying at a faster rate. However, no significant differences with respect to this phase of myocardial radiotracer washout for all the experiments was observed. Our working hypothesis is that this initial rapid clearance phase did not reflect viable cells but rather radioactivity directly injected into a blood vessel or emerging from the needle track due to myocardial contraction. For this reason, only the long component was used in our model to quantify viable cell activity. However, the short component may provide important data on cell retention in the evaluation of different transplantation methods.

Extrapolating our work to the clinic would be feasible with SPECT images acquired within hours of transplantation, approximately 2–3 d later, approximately 3–4 d later, and the final images acquired at approximately 5–7 times the effective half-life determined from the second and third measurements. Provided that the initial imaging included a whole-body scan, this would suggest both the fraction of the transplanted cells remaining in the myocardium immediately after transplantation and their survival half-life.

This study has several limitations. In establishing the accuracy of modeling cell survival in vivo, clearance data derived from canine experiments identified an upper and a lower limit. At the lower boundary, because of the variability in the DIRF measurement the model cannot account for half-lives faster than dead cell clearance kinetics (DIRF). Similarly, at the upper end, half-lives that are longer than leakage estimates cannot be corrected using this model.

Although this model assumes no cell division within the transplanted cell population and we cannot reliably predict cellular proliferation, our method does not rely on the absolute quantification of cell number. Rather, it relies on the $T^{l}_{1/2}$, suggesting that the rate at which ^{111}In signal is lost reflects changes in cell survival after corrections for death and leakage. Signal reductions would reflect the removal of ^{111}In from the injection site, as shown by a shorter $T^{l}_{1/2}$; the proliferation of healthy labeled cells, however, should result in the fractional sharing of the radiolabel without any loss, thus maintaining a constant signal.

After infarction, macrophages accumulate within the first 24 h, with numbers peaking around 7 d (*29*). Such macrophages within infarcted tissue could phagocytose released label and remain within the injection site; hence, DIRF could vary with time after infarction. However, our current results suggest otherwise, because all 4 animals treated with cells demonstrated extremely good fits to the last 3 data points ($r^2 = 0.96$–0.99). If DIRF changed dramatically with time after infarction, such excellent fits would be unlikely. Nevertheless, future work could evaluate macrophage effects on DIRF by injecting ^{111}In-labeled cellular debris at later times after infarction.

In a novel approach to estimate radiolabel leakage in vivo from cells that do not die, we labeled normal cardiomyocytes in situ. This may not accurately reflect leakage from transplanted BMSCs, because leakage potentially differs between different cell populations. However, we decided that in vitro–acquired leakage estimates to correct in vivo data as previously done (*27*) could not adequately account for in vivo biologic complexity.

Ex vivo validation will be important to confirm the accuracy of our model.

CONCLUSION

This work suggests that ^{111}In is a reliable marker of BMSC viability. We have shown in vitro that ^{111}In is highly retained in this cell population and does not show nonspecific uptake in surrounding cells. SPECT indirectly confirmed these findings in canine myocardium, demonstrating that ^{111}In-labeled cellular debris clearance is significantly faster than the clearance of ^{111}In from in situ–labeled cardiomyocytes. Using these results, we have mathematically modeled the time-dependent cell survival, which may predict the benefits of cell therapies or evaluate strategies to improve transplant cell survival.

ACKNOWLEDGMENTS

We thank Lela Deans, Dominique Ouimet, Jennifer Hadway, Eric Sabondjian, Yuan Jin, and Huafu Kong for technical assistance. We acknowledge funding from Canadian Institutes of Health Research (CIHR) (CIHR-MOP-9467), Ontario Research and Development Challenge Fund, Heart and Stroke Foundation of Ontario, and CIHR Vascular Training Program and an Ontario Graduate Scholarship in Science and Technology.

REFERENCES

1. Collins SD, Baffour R, Waksman R. Cell therapy in myocardial infarction. *Cardiovasc Revasc Med.* 2007;8:43–51.
2. Zhou R, Thomas DH, Qiao H, et al. In vivo detection of stem cells grafted in infarcted rat myocardium. *J Nucl Med.* 2005;46:816–822.
3. Chemaly ER, Yoneyama R, Frangioni JV, Hajjar RJ. Tracking stem cells in the cardiovascular system. *Trends Cardiovasc Med.* 2005;15:297–302.
4. Frangioni JV, Hajjar RJ. In vivo tracking of stem cells for clinical trials in cardiovascular disease. *Circulation.* 2004;110:3378–3383.
5. Kraitchman DL, Tatsumi M, Gilson WD, et al. Dynamic imaging of allogeneic mesenchymal stem cells trafficking to myocardial infarction. *Circulation.* 2005; 112:1451–1461.
6. Bengel FM. Nuclear imaging in cardiac cell therapy. *Heart Fail Rev.* 2006;11: 325–332.
7. Ott HC, McCue J, Taylor DA. Cell-based cardiovascular repair: the hurdles and the opportunities. *Basic Res Cardiol.* 2005;100:504–517.
8. Beeres SL, Bengel FM, Bartunek J, et al. Role of imaging in cardiac stem cell therapy. *J Am Coll Cardiol.* 2007;49:1137–1148.
9. Lim SY, Kim YS, Ahn Y, et al. The effects of mesenchymal stem cells transduced with Akt in a porcine myocardial infarction model. *Cardiovasc Res.* 2006;70:530–542.
10. Hou D, Youssef EA, Brinton TJ, et al. Radiolabeled cell distribution after intramyocardial, intracoronary, and interstitial retrograde coronary venous delivery: implications for current clinical trials. *Circulation.* 2005;112(9, suppl): I150–I156.

11. Freyman T, Polin G, Osman H, et al. A quantitative, randomized study evaluating three methods of mesenchymal stem cell delivery following myocardial infarction. *Eur Heart J.* 2006;27:1114–1122.
12. Hofmann M, Wollert KC, Meyer GP, et al. Monitoring of bone marrow cell homing into the infarcted human myocardium. *Circulation.* 2005;111:2198–2202.
13. Adonai N, Nguyen KN, Walsh J, et al. Ex vivo cell labeling with ^{64}Cu-pyruvaldehyde-bis(*N*4-methylthiosemicarbazone) for imaging cell trafficking in mice with positron-emission tomography. *Proc Natl Acad Sci USA.* 2002;99:3030–3035.
14. Thompson M, Wall DM, Hicks RJ, Prince HM. In vivo tracking for cell therapies. *Q J Nucl Med Mol Imaging.* 2005;49:339–348.
15. Shanthly N, Aruva MR, Zhang K, Mathew B, Thakur ML. Stem cells: a regenerative pharmaceutical. *Q J Nucl Med Mol Imaging.* 2006;50:205–216.
16. Jin Y, Kong H, Stodilka RZ, et al. Determining the minimum number of detectable cardiac-transplanted ^{111}In-tropolone-labelled bone-marrow-derived mesenchymal stem cells by SPECT. *Phys Med Biol.* 2005;50:4445–4455.
17. Itescu S, Schuster MD, Kocher AA. New directions in strategies using cell therapy for heart disease. *J Mol Med.* 2003;81:288–296.
18. Bicknell KA, Coxon CH, Brooks G. Can the cardiomyocyte cell cycle be reprogrammed? *J Mol Cell Cardiol.* 2007;42:706–721.
19. Reffelmann T, Kloner RA. Cellular cardiomyoplasty: cardiomyocytes, skeletal myoblasts, or stem cells for regenerating myocardium and treatment of heart failure? *Cardiovasc Res.* 2003;58:358–368.
20. Chien KR, Olson EN. Converging pathways and principles in heart development and disease: CV@CSH. *Cell.* 2002;110:153–162.
21. Byrne CL. Accelerating the EMML algorithm and related iterative algorithms by rescaled block-iterative methods. *IEEE Trans Image Process.* 1998;7:100–109.
22. Chin BB, Nakamoto Y, Bulte JW, Pittenger MF, Wahl R, Kraitchman DL. ^{111}In oxine labelled mesenchymal stem cell SPECT after intravenous administration in myocardial infarction. *Nucl Med Commun.* 2003;24:1149–1154.
23. Bindslev L, Haack-Sorensen M, Bisgaard K, et al. Labelling of human mesenchymal stem cells with indium-111 for SPECT imaging: effect on cell proliferation and differentiation. *Eur J Nucl Med Mol Imaging.* 2006;33:1171–1177.
24. Thakur ML, Segal AW, Louis L, Welch MJ, Hopkins J, Peters TJ. Indium-111-labeled cellular blood components: mechanism of labeling and intracellular location in human neutrophils. *J Nucl Med.* 1977;18:1022–1026.
25. Chen P, Wang J, Hope K, et al. Nuclear localizing sequences promote nuclear translocation and enhance the radiotoxicity of the anti-CD33 monoclonal antibody HuM195 labeled with ^{111}In in human myeloid leukemia cells. *J Nucl Med.* 2006;47:827–836.
26. Reilly RM, Kiarash R, Cameron RG, et al. ^{111}In-labeled EGF is selectively radiotoxic to human breast cancer cells overexpressing EGFR. *J Nucl Med.* 2000;41:429–438.
27. Tran N, Li Y, Maskali F, et al. Short-term heart retention and distribution of intramyocardial delivered mesenchymal cells within necrotic or intact myocardium. *Cell Transplant.* 2006;15:351–358.
28. Ballinger JR, Gnanasegaran G. Radiolabelled leukocytes for imaging inflammation: how radiochemistry affects clinical use. *Q J Nucl Med Mol Imaging.* 2005;49:308–318.
29. Dewald O, Ren G, Duerr GD, et al. Of mice and dogs: species-specific differences in the inflammatory response following myocardial infarction. *Am J Pathol.* 2004;164:665–677.